ACS OMEGA

Open Access

http://pubs.acs.org/journal/acsodf

Article

First-Principles Predictions of MoS_2-WS_2 In-Plane Heterostructures for Sensing Dissolved Gas Species in Oil-Immersed Transformers

Tian Tian, Xiu Zhou,* Jiaying Yu, Jin Bai, Lei Chen, Ninghui He, Xiuguang Li, Heng Zhang, and Hao Cui*

Cite This: *ACS Omega* 2024, 9, 20253−20262

Read Online

ACCESS | Metrics & More | Article Recommendations | Supporting Information

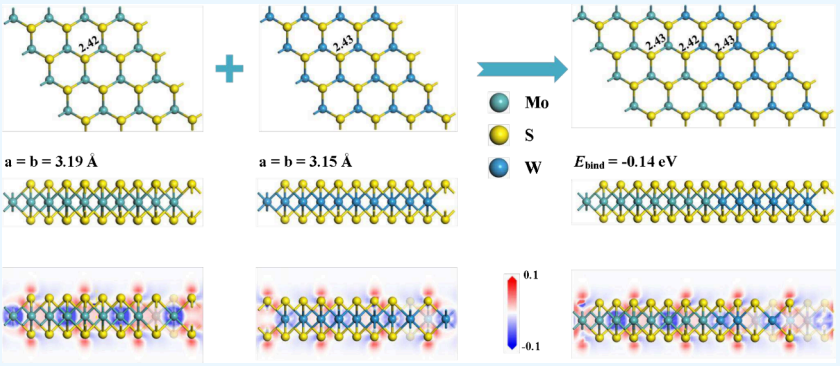

ABSTRACT: This work from first-principles insight uses a MoS_2-WS_2 in-plane heterostructure as a potential sensing material for detection of CO and C_2H_2, two typical dissolved gases in oil-immersed transformers, in order to evaluate the operation status. The adsorption performance of the MoS_2-WS_2 heterostructure upon two gas species is assessed via three adsorption sites and compared with isolated MoS_2 and WS_2. Results indicate that MoS_2-WS_2 performs with a much stronger binding force and charge-transfer for adsorptions of CO and C_2H_2 in comparison to the isolated counterpart, which gives rise to more obvious deformation in the electronic property of MoS_2-WS_2 as well as a much larger resistance-based sensing response. The recovery time of MoS_2-WS_2 for desorption of CO and C_2H_2 molecules is also appropriate to allow the reusability of such a sensor. The findings in this work uncover the admirable sensing potential of transition metal dichalcogenides (TMDs)-based heterostructures upon oil dissolved gases, which opens up a new way to explore novel 2D nanomaterials as resistive gas sensors for dissolved gas analysis in electrical oil-immersed transformers.

1. INTRODUCTION

Nowadays, oil-immersed electrical transformers play a remarkable role in the urban distribution network to transmit electricity and ensure the good operation of the whole power system.[1,2] To guarantee the insulation properties of the electrical transformers, mineral oil is filled inside the devices as the insulation medium, undergoing possible partial discharge as well as some other insulation defects.[3,4] In a long running, the partial discharge can decompose the insulation oil into several gas species including CO and C_2H_2, and these gases will dissolve in the oil, forming bubbles.[5,6] It has been reported that the generated gas species would impair the insulation performance of the mineral oil, thus threatening the working condition of oil-immersed electrical transformers.[7,8] Therefore, scholars in this field use dissolved gas analysis to evaluate the operating condition of oil-immersed transformers.[9] Specifically, the dissolved gases should be extracted from the mineral oil initially and be detected using certain gas sensing methods, and finally possible insulation defects and the severity of electrical transformers could be identified.[10] In these decades, dissolved gas analysis has largely been developed and and in a workable manner to realize operation status evaluation for oil-immersed transformers, and the kernel of such method is to explore an effective and highly sensitive gas sensing method to accurately determine typical gases in the oil,[11] so as to evaluate the operational status of oil-immersed transformers.[12]

For the end of gas detection, nanomaterial-based gas sensors have the advantages of easy operation, low cost, small size, and high sensitivity in comparison with gas spectrum technology,[13,14] and thus the nanosensor method has experienced significant developments for gas detection in recent years,

Received: January 21, 2024
Revised: March 16, 2024
Accepted: March 20, 2024
Published: April 23, 2024

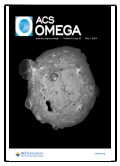

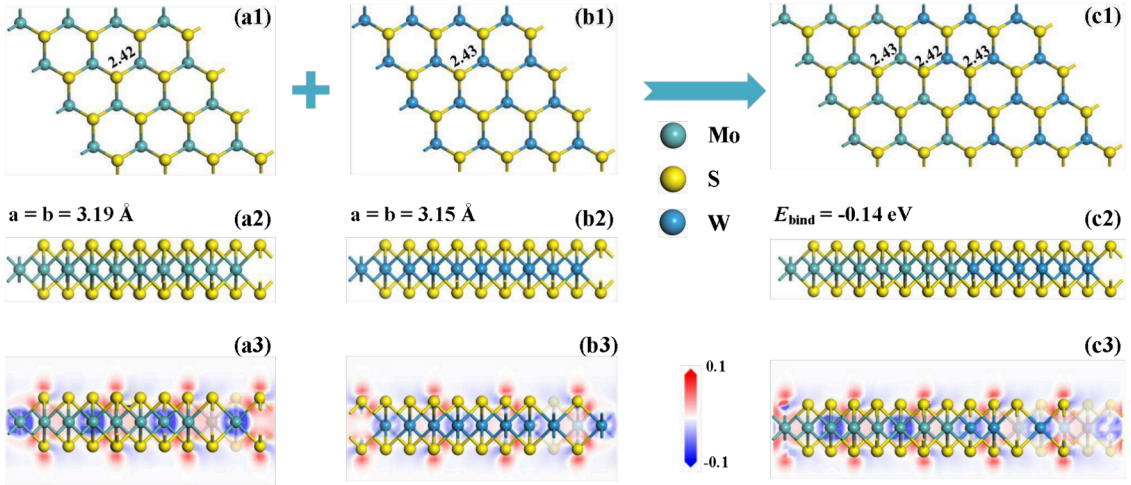

Figure 1. Morphology and DCD of (a1−a3) pristine MoS_2 monolayer, (b1−b3) pristine WS_2 monolayer, and (c1−c3) MoS_2-WS_2 heterojunction. In DCD, the red areas are electron accumulation, and the blue areas are electron depletion with the isosurface ranging from −01 to 0.1 e/Å^2. The black values are the bond length, unit in Å.

especially for those gas sensing materials using two-dimensional (2D) materials.[15−18] Nowadays, the transition metal dichalcogenides (TMDs) are theoretically and experimentally investigated with admirable sensitivity and a rapid response for the exploration of gas-sensing devices.[19−21] For example, MoX_2 and WX_2 (X = S, Se and Te) are explored for gas sensing applications for several typical gas species,[22−24] which can provide more favorable sensing responses compared to carbon-based materials and metal oxide semiconductors,[25] which paves the way for their further investigations in the field of gas sensing.[26,27]

Meanwhile, TMDs heterostructures in recent years have also been discovered and have been synthesized for many applications.[28−30] For example, Xu et al. report the ambient pressure chemical vapor deposition process to synthesize a MoS_2-WS_2 in-plane heterostructure, with $(NH_4)_6Mo_7O_{24}\cdot 4H_2O$ and $(NH_4)_{10}W_{12}O_{41}\cdot xH_2O$ as Mo and W sources.[31] Sharma et al. report a novel method to synthesize a large area and patterned growth of MoS_2-WS_2 heterostructures for applications in the fields of nano- and opt-electronics.[32] At the same time, there are several recent investigations about MoS_2-WS_2 heterostructures for explorations as typical gas sensors. For instance, Ikram et al. synthesized a MoS_2@WS_2 heterojunction with a large-surface area and ultrasensitivity for detection of NO_2 at room temperature.[33] Zhang et al. from experimental aspects report the high-sensitivity performance of MoS_2/WS_2 heterojunctions upon NH_3 for gas sensor exploration as well.[34] On the other hand, there is limited investigation from the theoretical aspects to investigate the gas sensing potential of MoS_2-WS-WS_2 heterostructures. Therefore, we think that the simulations of MoS_2-WS_2 heterostructures upon the gas adsorption and sensing performances should be conducted to help understand the geometric and electronic properties of such heterojunctions and explore novel applications in the gas sensing field.

In this work, we used the first-principles theory to establish the MoS_2-WS_2 heterostructure and analyze its physicochemical properties, followed by the analysis of its gas adsorption and sensing behaviors upon two typical dissolved gases, namely CO and C_2H_2, to explore the gas sensing potential of MoS_2-WS_2 heterostructures for dissolved gas analysis in oil-immersed transformers. The adsorption parameters, electronic properties, as well as the recovery properties of the MoS_2-WS_2 heterostructure upon two gas species are well-analyzed in this work. We believe that the findings herein can not only shed light on the physicochemical properties of TMD heterojunctions but also can help design novel heterojunction-based gas sensors in this field.

2. COMPUTATIONAL DETAILS

The first-principles simulations were conducted in the DMol^3 package,[35,36] in which the exchange correction relationship in the geometric optimization and electronic calculations were addressed by the Perdew−Burke−Ernzerhof (PBE) function.[37] To better understand the van der Waals force and long-range reactions, we selected the DFT-D2 method raised by Tkatchenko and Scheffler to cope with the dispersion corrections.[38] In the Brillouin-zone, a 10 × 10 × 1 k-point was defined in the grid to perform the geometric and electronic simulations.[39] Apart from that, the geometries were optimized under an energy convergence accuracy of 10^{-5} Ha, and the global orbital cutoff radius of 5.0 Å was determined to address the metal atoms.[40]

To establish the MoS_2-WS_2 heterojunction, the 3 × 3 × 1 supercell of the MoS_2 and WS_2 monolayers was modeled first. Also, we established a vacuum region of 20 Å along the z direction of the heterojunction to prevent the possible surface interactions between the adjacent units in the gas adsorptions.[41] In the calculations of the band structure, the empty bands are set as 12. Moreover, we adopted Hirshfeld population analysis to consider the charge-transfer (Q_T) in the gas-surface interactions, by which one could determine that the positive value suggested the electron-donating properties of the adsorbed gas species, whereas the negative value suggested their electron-accepting properties.

3. RESULTS AND DISCUSSION

3.1. Properties of MoS_2-WS_2 Heterostructures. To understand the geometric and electronic properties of the MoS_2-WS_2 in-plane heterojunction, we establish and geometrically optimize the structures of pristine MoS_2 and WS_2 monolayers for better comparison, with their optimized morphologies and the deformation charge density (DCD)

https://doi.org/10.1021/acsomega.4c00681
ACS Omega 2024, 9, 20253−20262

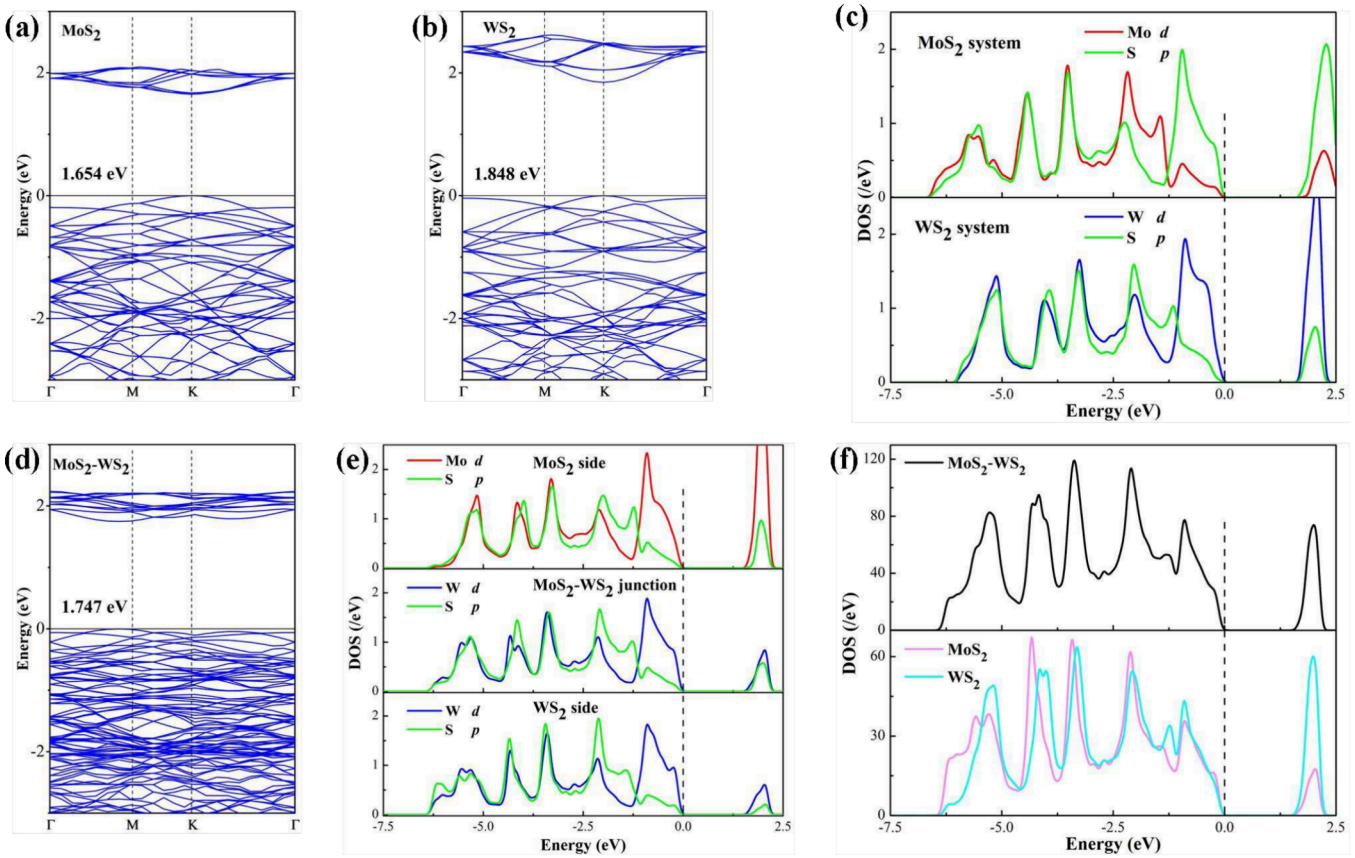

Figure 2. Exhibition of electron properties. (a), (b), and (d) band structure of pristine MoS_2, WS_2, and MoS_2-WS_2 systems; (c) and (e) orbital DOS of bonded atoms and (f) total and partial DOS in the MoS_2-WS_2 system. In the band structure, the black values are the bandgap of related systems, and in DOS the dashed line is the Fermi level, which is the default set of the top valence band.

plotted in Figure 1. Besides, in order to evaluate the binding force between the MoS_2 and WS_2 monolayer, we determined the binding energy (E_{bind}) calculated by

$$E_{bind} = E_{MoS_2\text{-}WS_2} - E_{MoS_2} - E_{WS_2} \quad (1)$$

wherein the $E_{MoS_2\text{-}WS_2}$, E_{MoS_2}, and E_{WS_2} suggest the total energy of the MoS_2-WS_2 in-plane heterojunction, pristine MoS_2 and WS_2 monolayer.

One can see from Figure 1(a1−a2) and (b1−b2) that lattice constants of the pristine MoS_2 and WS_2 monolayer are obtained to be 3.19 and 3.15 Å, in which the Mo−S and W−S bond lengths are measured to be 2.43 and 2.42 Å, respectively. These findings are in good consistency with the previous references,[42,43] and the slightly larger lattice constant and bond length in the MoS_2 system may be attributed to the larger atomic radii of the Mo atom (1.38 Å) compared with the W atom (1.37 Å) in the WS_2 system.[44] Besides, we should note that the small difference in their lattice constants indicates the good matching ratio of the MoS_2 and WS_2 monolayer, which can give rise to a favorable heterojunction structure.[45] Upon the MoS_2-WS_2 heterojunction, one can see in Figure 1(c1−c2) that the Mo−S bond on the MoS_2 side and W−S bond on WS_2 side are measured to be equal to 2.43 Å, and the Mo−S bond on the MoS_2−WS_2 junction is measured to be 2.42 Å, which indicates the slight but still favorable binding force between the Mo and S atoms at the site of heterojunction.[45] Apart from that, the E_{bind} for the heterojunction is calculated to be −0.14 eV, which confirms the weak interaction between the MoS_2 and WS_2 surface and the energy-favorable property that could occur spontaneously during the formation of the heterojunction. Furthermore, we perform the molecular dynamic simulation under 300 K for 2000 steps (1 fs for one step) to verify the thermostability of the MoS_2-WS_2 configuration, with the energy and temperature fluctuation and the optimized structure exhibited in Figure S1. It is found that the geometric structure of the MoS_2-WS_2 heterostructure experiences slight deformation after dynamic simulations with the temperature fluctuation varying from 150 to 750 °C. Apart from that, the energy of the MoS_2-WS_2 heterostructure suffers little change within 0.001 Ha (0.027 eV) in the temperature fluctuations. These findings indicate the good thermostability and geometric stability of the MoS_2-WS_2 heterostructure. Also, the frequencies of the MoS_2-WS_2 heterostructure after dynamic simulations based on the vibrational analysis range from 89.7 to 883.89 cm^{-1}, which confirms the good chemical stability of such configuration.

From the DCD of MoS_2, WS_2, and MoS_2-WS_2 systems in Figure 1(a3−c3), it is seen that the electron accumulations are on the S atoms, and the electron depletion are on the Mo or W atoms, which agrees with their electronegativity.[46] Specifically, according to the Hirshfeld analysis, the Mo and S atoms in the MoS_2 monolayer are charged by 0.226 and −0.113 e, and the W and S atoms in the WS_2 monolayer are charged by 0.126 and −0.063 e. These findings agree with the weaker electronegativity of the Mo atom compared with the W atom, which leads to the stronger electron-donating properties of the Mo atom.[46] Meanwhile, the MoS_2 monolayer as a whole donates 0.188 e to the WS_2 monolayer in the MoS_2-WS_2

https://doi.org/10.1021/acsomega.4c00681
ACS Omega 2024, 9, 20253−20262

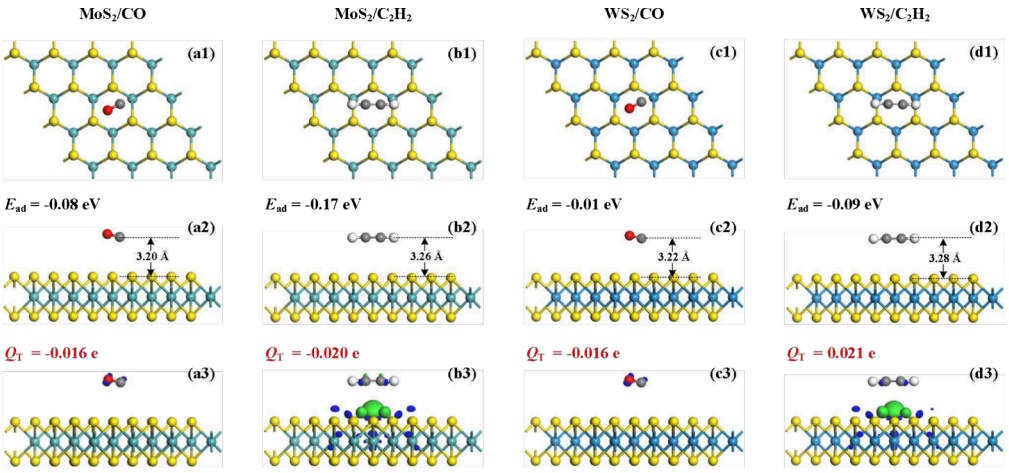

Figure 3. MPC and CDD of CO and C_2H_2 adsorptions on the MoS_2 and WS_2 surfaces. (a1−a3) MoS_2/CO system, (b1−b3) MoS_2/C_2H_2 system, (c1−c3) WS_2/CO system, and (d1−d3) WS_2/C_2H_2 system. In CDD, the blue areas are electron accumulation, the green areas are electron depletion, and the isosurface is set as 0.002 e/Å^3.

heterojunction, further confirming the stronger electronegativity of the W atom. That is, the WS_2 becomes the electron localization in the MoS_2-WS_2 heterostructure.

Figure 2 exhibits the band structure, total density of state (DOS), and orbital DOS of the pristine MoS_2, WS_2, and MoS_2-WS_2 systems to understand their electronic properties, especially the comparison between the heterostructure and the pristine surfaces. One can see from the band structure of pristine MoS_2 and WS_2 monolayer in Figure 2(a−b) that their bandgap are obtained as 1.654 and 1.848 eV, respectively. Apart from that, the top valence band and bottom conduction band of the MoS_2 and WS_2 systems are both located at the K point, indicating their direct semiconducting properties. These findings are in good accordance with the previous reports,[47,48] suggesting the good accuracy of our calculations. In the orbital DOS of MoS_2 and WS_2 systems Figure 2(c), the S *p* orbital is highly hybrid with the Mo *d* and W *d* orbitals, which indicates the favorable binding force in the Mo−S and W−S bonds. For the band structure of MoS_2-WS_2 heterojunction in Figure 2(d), it is found that that the bandgap is calculated to be 1.747 eV, which is smaller than that of WS_2 but larger than that of MoS_2, and the top valence band and bottom conduction band are both at the M point, indicating that the in-plane heterojunction between MoS_2 and WS_2 does not impact their direct semiconducting properties. Also, we plot the orbital DOS of the bonded atoms in Figure 2(e) for the MoS_2-WS_2 system, namely the Mo *d* and S *p* orbital in the MoS_2 side, the W *d* and S *p* orbitals in the WS_2 side, and the W *d* and S *p* orbitals in the MoS_2-WS_2 junction. From the orbital DOS, it could be found that (i) the Mo *d* and S *p* orbitals in the MoS_2 side as well as the W *d* and S *p* orbitals in the WS_2 side hybridize highly accounting for their good binding nature, and (ii) the W *d* and S *p* orbitals in the MoS_2-WS_2 junction hybridize strongly as well, even stronger than those in the WS_2 site considering the larger overlapped area between two orbitals (for example at 2.0 eV) in the former systems. Such finding confirms the admirable binding force between the MoS_2 and WS_2 when they form the in-plane heterojunction. According to the total DOS in Figure 2(f), we can see that the WS_2 contributes significantly more in comparison with the MoS_2 in the MoS_2-WS_2 system, especially around the Fermi level wherein the electronic states of the WS_2 are much stronger than MoS_2, which may be attributed to the orbital interaction and electronic contributions of the W−S bonds in the junctions. All these analyses reveal the admirable chemical reactivity and electron mobility between the MoS_2 and WS_2 in the MoS_2-WS_2 system.

3.2. Gas Adsorption on MoS_2, WS_2, and MoS_2-WS_2 Heterostructures. With the geometric understandings of MoS_2, WS_2, and MoS_2-WS_2 heterostructure, their adsorption behaviors upon CO and C_2H_2, two typical dissolved gases, are investigated by putting the CO and C_2H_2 molecules onto the nanosurfaces through three possible adsorption sites, traced as T_S (at the top of S atom), T_X (at the top of W or Mo atom), and T_H (at the top of the hollow site) with the initial atomic distance of about 2.5 Å, to conduct the geometric optimizations. Then, the most preferred configurations (MPC) for gas adsorption should be determined for further analysis, which is determined as the configuration with the most negative adsorption energy (E_{ad}) of the nanosurface upon the gas molecule, and by such definition the E_{ad} is calculated by

$$E_{ad} = E_{surface/gas} - E_{surface} - E_{gas} \quad (2)$$

wherein $E_{surface/gas}$ indicates the total energy of gas adsorbed MoS_2, WS_2, or MoS_2-WS_2, $E_{surface}$ indicates the total energy of the nanosurface, namely MoS_2, WS_2, or MoS_2-WS_2, and E_{gas} is the total energy of the isolated gas molecule. By eq 2, the MPC for CO and C_2H_2 molecule adsorption onto the three nanosurfaces could be determined, and the charge density difference (CDD) is plotted for the MPC to better understand the charge-transfer behavior and binding force between the nanosurface and the gas species. For better comparison, Figure 3 plots the MPC and CDD of CO and C_2H_2 adsorptions onto the MoS_2 and WS_2 surfaces.

For CO and C_2H_2 adsorption onto the MoS_2 monolayer in Figure 3(a−b), it could be seen that the CO molecule is basically parallel with the MoS_2 surface with a small slope, the C_2H_2 molecule is fully parallel with the MoS_2 surface, and the molecule−surface distances are obtained as 3.20 and 3.26 Å for two systems, respectively. Such long distances imply the weak interaction between the MoS_2 and two gas species, and accordingly there is no formation of a new bond between them. According to the definition of adsorption energy, the E_{ad} values in CO and C_2H_2 adsorbed MoS_2 systems are calculated

https://doi.org/10.1021/acsomega.4c00681
ACS Omega 2024, 9, 20253−20262

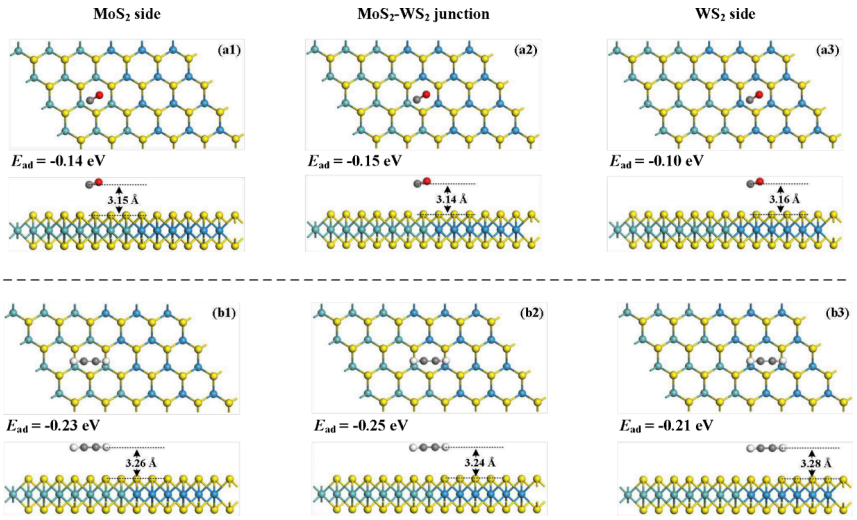

Figure 4. MPC for CO and C_2H_2 adsorptions on the MoS_2-WS_2 surfaces. (a1−a3) CO system and (b1−b3) C_2H_2 system.

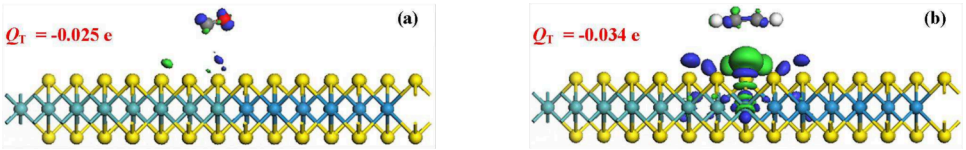

Figure 5. CDD of CO and C_2H_2 adsorptions on the MoS_2-WS_2 junction site. (a) CO system and (b) C_2H_2 system. The blue areas are electron accumulation, the green areas are electron depletion, and the isosurface is set as 0.002 e/Å^3.

as −0.08 and −0.17 eV, respectively. Such small absolute values of E_{ads} in these two systems indicate the physisorption, in which the van der Waals' force plays the dominant role in the gas-surface interactions.[49] From the CDD of two systems, one can see that there is some electron accumulation on the CO and C_2H_2 molecules, which implies their electron-accepting property when interacting with the MoS_2 surface. Besides, there also exists some electron depletion besides the MoS_2 surface in the C_2H_2 system, which indicates (i) the electron-losing property of the nanosurface and (ii) the stronger charge-transfer behavior here in comparison with the CO system. These findings are consistent with those based on the Hirshfeld population analysis, which reveals that the CO and C_2H_2 molecules are respectively charged by −0.016 and −0.020 e, and from the quantitative manner it reveals the charge-transfer path from the MoS_2 to two such gas molecules and the stronger electron-accepting property of the C_2H_2 molecule than the CO molecule.

In terms of CO and C_2H_2 adsorptions onto the WS_2 monolayer, in Figure 3(c−d), one could find that the adsorption configurations, including the adsorption site and molecular orientation, of two such systems are similar to those on the MoS_2 monolayer. However, the molecule−surface distances in the WS_2/gas systems are somewhat longer than those in the MoS_2/gas systems obtained as 3.22 Å in the CO system and 3.28 Å in the C_2H_2 system, which implies the weaker adsorption performance of WS_2 compared with MoS_2 upon two gas molecules. Such an assumption could be verified by the calculation of E_{ad}, which herein are obtained as −0.01 and −0.09 eV, respectively. From this aspect, the physisorption could also be identified for CO and C_2H_2 adsorption onto the WS_2 monolayer. Meanwhile, the CDD distributions in the WS_2/gas systems are similar to those of the MoS_2/gas systems, and we will not give details here. Moreover, the charge-transfer behavior in the WS_2/gas systems is also the same as those in the MoS_2/gas systems wherein the CO and C_2H_2 both show an electron-accepting property withdrawing 0.016 and 0.021 e from the WS_2 surface.

Following the CO and C_2H_2 adsorptions onto the MoS_2-WS_2 heterostructure, here we consider three possible adsorption sites, namely onto the MoS_2 side, the MoS_2-WS_2 junction, and the WS_2 side, with the MPC of three adsorption sites plotted in Figure 4. From this figure, we can see that the CO and C_2H_2 adsorption configurations onto the MoS_2-WS_2 surface are quite similar as that on the MoS_2 or WS_2 surface, no matter on the MoS_2 side, WS_2 side, or above MoS_2-WS_2 junction. The difference is that on the MoS_2-WS_2 the molecule−surface distance gets slightly shorter in comparison with those on the MoS_2 or WS_2 surface. Specifically, the shortest molecule−surface distance in the CO adsorbed systems is on the MoS_2-WS_2 junction (3.14 Å), followed by the MoS_2 side (3.15 Å) and the longest one being the WS_2 side (3.16 Å), whereas that in the C_2H_2 adsorbed systems is in the order as MoS_2-WS_2 junction (3.24 Å) < MoS_2 side (3.26 Å) < WS_2 side (3.28 Å). According to the calculations of E_{ad}, we can infer that the MPC for CO and C_2H_2 adsorptions on the MoS_2-WS_2 heterostructure is on the MoS_2-WS_2 junction, with the E_{ad} of −0.15 and −0.25 eV, respectively. At the same time, it should be noted that for CO and C_2H_2 adsorptions on the MoS_2-WS_2 heterostructure through the MoS_2 side (−0.14 and −0.23 eV) and WS_2 side (−0.10 and −0.21 eV), the E_{ads} are also comparable and within small differences with that on through the MoS_2-WS_2 junction; besides, these E_{ads} values indicate that the adsorption performance of the MoS_2-WS_2 heterostructure upon CO and C_2H_2 molecules is stronger than those of MoS_2 and WS_2. In other words, the heterostructure between MoS_2 and WS_2 can enhance their gas adsorption performance, especially on the junction site.

https://doi.org/10.1021/acsomega.4c00681
ACS Omega 2024, 9, 20253−20262

Figure 5 exhibits the CDD for CO and C_2H_2 adsorptions onto the junction of the MoS_2-WS_2 heterostructure, namely the MPC of the gas adsorption systems. One can see in this figure that the electron accumulations are dominantly located at the CO and C_2H_2 molecule, suggesting their electron-withdrawing property interacting with the MoS_2-WS_2 heterojunction, and the electron density in the area between the gas species and the nanosurface is much denser than those on the MoS_2 or WS_2 systems, indicating the stronger electron-donating property of the MoS_2-WS_2 heterojunction transferring electron the gas species. Based on Hirshfeld population analysis, we could find that the CO and C_2H_2 molecules on the MoS_2-WS_2 surface is negatively charged by 0.025 and 0.034 e, respectively. These confirm the larger amount of charge-transfer from the MoS_2-WS_2 surface to the gas species in comparison with those from the MoS_2 or WS_2 surface. In other words, the MoS_2-WS_2 surface has stronger reactivity and electron mobility than the isolated MoS_2 or WS_2 surface,[34] and the CO and C_2H_2 molecule still act as the electron acceptor, which may be attributed to their reducibility nature.[50]

Furthermore, to make the E_{ad} of the gas adsorbed systems more convincing, we calculated the values with dipole correction and zero-point energy correction as listed in Table 1. It could be found from this table that the calculated

Table 1. E_{ad} of Adsorbed Systems with Dipole Correction and Zero-Point Energy Correction

systems	E_{ad} (eV)	E_{ad} with dipole correction (eV)	E_{ad} with zero-point energy correction (eV)
MoS_2/CO	−0.08	$-0.08-4.8 \times 10^{-5}$	$-0.08-1.5 \times 10^{-4}$
MoS_2/C_2H_2	−0.17	$-0.17-3.1 \times 10^{-5}$	$-0.17-1.2 \times 10^{-4}$
WS_2/CO	−0.01	$-0.01-2.6 \times 10^{-5}$	$-0.01-5.2 \times 10^{-4}$
WS_2/C_2H_2	−0.09	$-0.09-4.3 \times 10^{-5}$	$-0.09-8.1 \times 10^{-5}$
MoS_2-WS_2/CO	−0.15	$-0.15-2.2 \times 10^{-5}$	$-0.15-5.3 \times 10^{-5}$
MoS_2-WS_2/C_2H_2	−0.25	$-0.25-2.0 \times 10^{-5}$	$-0.25-1.9 \times 10^{-4}$

E_{ad} values with two such corrections have no big differences with those without considering the correction. That is, the dipole correction and zero-point energy correction have quite a small impact on the adsorption performance of the MoS_2, WS_2, and MoS_2-WS_2 surfaces upon CO and C_2H_2 molecules. These findings verify the good accuracy of the current set to obtain the adsorption energies. For a short summary, the MoS_2-WS_2 heterostructure has enhanced adsorption performance upon CO and C_2H_2 compared with the isolated MoS_2 or WS_2 surface, giving rise to the more absolute value of adsorption energy and a larger amount of charge-transfer from the nanosurface to the gas molecules. From this aspect, one can assume that the heterojunction is a workable manner to promote the gas adsorption behavior for the isolated counterpart. However, considering that the absolute value of E_{ads} in the CO or C_2H_2 adsorbed MoS_2-WS_2 systems is not larger than the critical value of 0.8 eV,[51] we would like to mention that MoS_2-WS_2 also shows physisorption upon two typical dissolved gas molecules, with a stronger performance upon C_2H_2 other than CO.

3.3. Band Structure Analysis and Gas Sensor Exploration. With the verified assumption that the MoS_2-WS_2 heterostructure shows a stronger adsorption performance upon CO and C_2H_2, two typical dissolved gas species in the electrical transformer oil, in comparison with the isolated MoS_2 or WS_2, one can assume that the MoS_2-WS_2 may have the potential to be explored as a gas sensor with the improved sensing behavior to realize dissolved gas detection. For this end, the band structure of the gas adsorbed MoS_2-WS_2 systems is plotted in Figure 6, in which the band structure for the gas adsorbed MoS_2 or WS_2 systems is exhibited and compared to better understand the remarkable electronic deformation in the MoS_2-WS_2 system by CO and C_2H_2 adsorptions. Moreover, the bandgap of these gas adsorbed systems and the changing rate from the isolated nanosurface to the gas adsorbed counterparts are listed in Table 2.

From the band structure distributions of gas adsorbed MoS_2 and WS_2 systems, one can see that the bandgap of the MoS_2 is reduced to 1.651 eV after CO adsorption and to 1.645 eV after C_2H_2 adsorption, while that of the WS_2 is increased equally to 1.864 eV after CO and C_2H_2 adsorptions. That is, the bandgap of the MoS_2 is reduced by 0.18% in the CO system and by 0.54% in the C_2H_2 system, and that of the WS_2 is increased by equally 0.87% in the CO and C_2H_2 systems. Although the change of bandgap after gas adsorptions can modulate the electrical conductivity of MoS_2 or WS_2, these small changes may not give rise to a remarkable or obvious electrical response for sensitive detections.[52] On the other hand, the bandgap of the MoS_2-WS_2 heterostructure is reduced to be 1.486 eV (by 14.94%) after adsorption of CO molecule and to be 1.352 eV (by 22.71%) after adsorption of the C_2H_2 molecule. One can calculate that the changing rates of the bandgap in the gas adsorbed MoS_2-WS_2 systems are several times compared with those in the gas adsorbed MoS_2 or WS_2 systems (for CO: 82.4 times than MoS_2 and 17.2 times than WS_2; for C_2H_2: 42.1 times than MoS_2 and 26.1 times than WS_2). Therefore, the change in electrical conductivity of the MoS_2-WS_2 heterostructure after gas adsorption could be much larger and would be feasibly detected for sensitive CO and C_2H_2 detection, giving rise to a much higher sensing response accordingly (detailed analysis could be found below). One thing we would like to mention is that in all gas adsorbed systems, the top valence band and bottom conduction band are located at the same point, indicating that gas adsorptions have no impact on the direct semiconducting property of isolated MoS_2 and WS_2, as well as the MoS_2-WS_2 heterostructure.

As reported, the change of electrical conductivity (resistance) of the nanomaterial provides the basic sensing mechanism to be explored as a resistive gas sensor,[53] as the electrical conductivity (σ) of the nanosurface is related to its bandgap (B_g) as expressed in eq 3:[54]

$$\sigma = \lambda \cdot e^{(-B_g/2kT)} \tag{3}$$

wherein λ is a constant, T is temperature, and k is the Boltzmann constant (1.38×10^{-23} J/K).[55] From this equation, we could conclude that the electrical resistance of the MoS_2 and MoS_2-WS_2 would be reduced after CO and C_2H_2 adsorptions, whereas that of the WS_2 would be increased after CO and C_2H_2 adsorptions. Moreover, based on the changed electrical conductivity in the nanosurface, the sensing response (S) of such nanomaterial-based gas sensor can be calculated by[56]

$$S = ({\sigma_{gas}}^{-1} - {\sigma_{pure}}^{-1})/{\sigma_{pure}}^{-1} \tag{4}$$

in which σ_{gas} and σ_{pure} separated indicate the electrical conductivity of the gas adsorbed nanosurface and the isolated nanomaterial (namely isolated MoS_2, WS_2, and MoS_2-WS_2 in

https://doi.org/10.1021/acsomega.4c00681
ACS Omega 2024, 9, 20253−20262

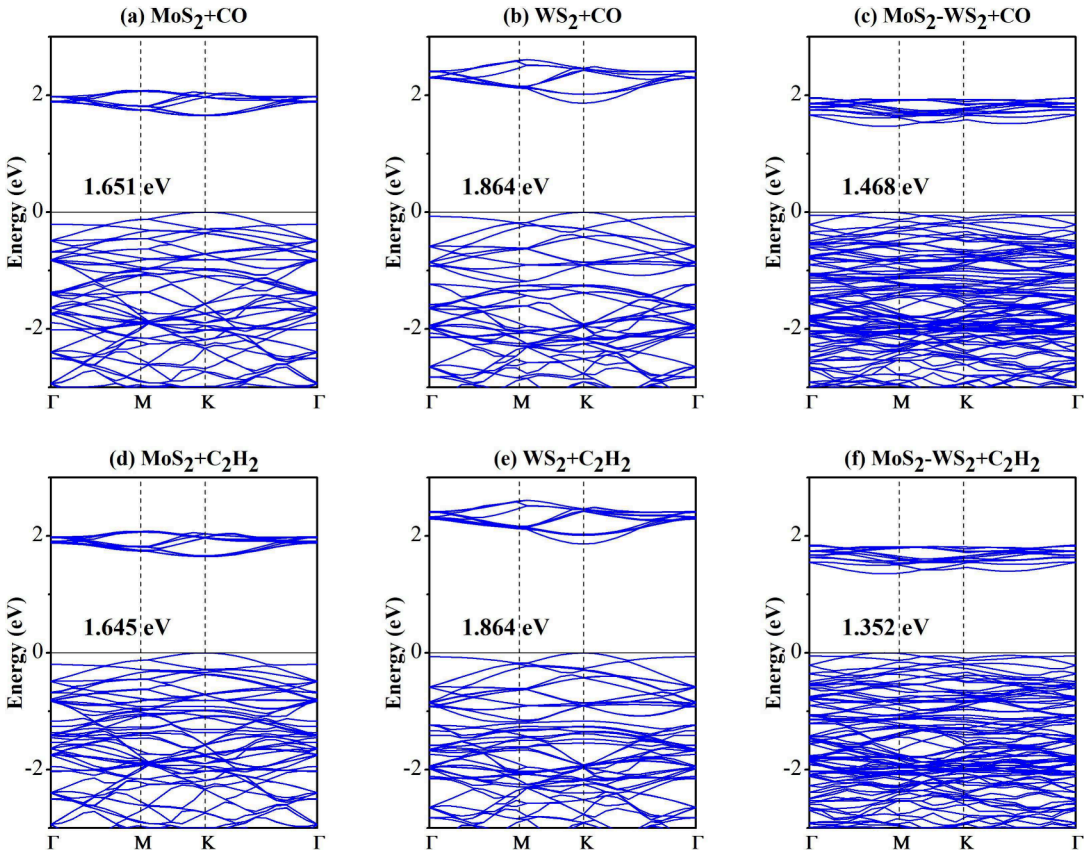

Figure 6. Band structure of gas adsorbed systems. (a−c) CO adsorbed MoS_2, WS_2, and MoS_2-WS_2 system and (d−f) C_2H_2 adsorbed MoS_2, WS_2, and MoS_2-WS_2 system, and the black values are the bandgap.

Table 2. Bandgap and Changing Rate of Gas Adsorbed MoS_2, WS_2 and MoS_2-WS_2 Systems

	CO system		C_2H_2 system	
nanosurface (bandgap, eV)	bandgap (eV)	changing rate	bandgap (eV)	changing rate
MoS_2 (1.654)	1.651	−0.18%	1.645	−0.54%
WS_2 (1.848)	1.864	+0.87%	1.864	+0.87%
MoS_2-WS_2 (1.747)	1.486	−14.94%	1.352	−22.71%

this work). According to eq 3 and 4, the sensing responses of MoS_2, WS_2, and MoS_2-WS_2 for CO and C_2H_2 detection at room temperature (298 K) are displayed in Figure 7.

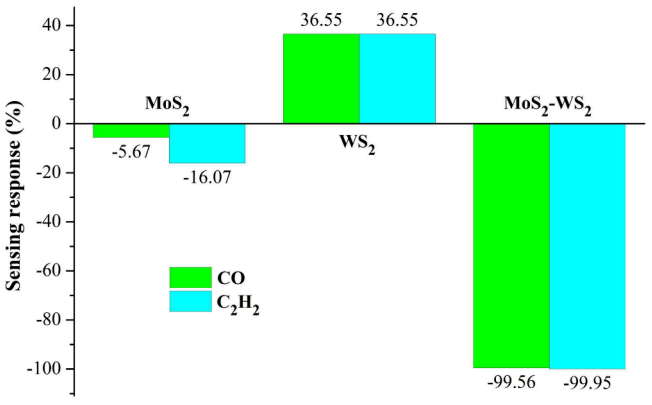

Figure 7. Sensing response of MoS_2, WS_2, and MoS_2-WS_2 upon CO and C_2H_2 at room temperature.

From this figure, we can see that MoS_2 and MoS_2-WS_2 have negative sensing responses upon CO and C_2H_2, while WS_2 has a positive sensing response upon two gas molecules. For details, the sensing response of −5.67% and −16.07% are obtained for detection of CO and C_2H_2 using the MoS_2-based gas sensor. However, such a sensing response is somewhat small, and the change may not be feasibly detected and checked by the principle computer. Using the WS_2-based gas sensor, the sensing responses upon CO and C_2H_2 are calculated equally as 36.55%. Such values are moderate for gas detection, and thus one can assume that WS_2 has a certain potential to be explored as a resistive gas sensor for detection of typical dissolved gases. Moreover, the sensing responses in the CO and C_2H_2 adsorbed MoS_2-WS_2 systems are obtained as −99.56% and −99.95%, respectively, which indicates that the electrical resistance of the MoS_2-WS_2 would be sharply reduced by almost one time after adsorption of the CO or C_2H_2 molecule. This reveals the strong potential of MoS_2-WS_2 for exploration of a resistive gas sensor upon two such species, with much promoted sensing response in comparison with MoS_2 or WS_2. We need to highlight that the sensing response obtained in the current work from the calculations of equations may not be quite consistent and equivalent with the experiment findings. However, it provides the basic sensing mechanism and rough sensing response of the nanosurfaces, which is meaningful to provide guidance for further experiments.

Moreover, to investigate the reusability of the MoS_2-WS_2 for sensing CO and C_2H_2 gases, the recovery time (τ) for their

https://doi.org/10.1021/acsomega.4c00681
ACS Omega 2024, 9, 20253−20262

desorption from the MoS_2-WS_2 surface is calculated based on the van't-Hoff-Arrhenius theory,[57] as calculated by

$$\tau = A^{-1}e^{(-E_{ad}/kT)} \quad (5)$$

in which A is attempt frequency (10^{12} s^{-1}),[58] k is Boltzmann constant, and T is temperature. From eq 5, the required times for CO and C_2H_2 desorption from the MoS_2-WS_2 heterostructure at room temperature (298 K) are obtained as 0.34 and 16.84 ns, respectively. These findings manifest the good recovery property of the 3 × 5 × 1 MoS_2-WS_2 supercell for desorption of one gas molecule from its surface, and therefore one can assume that MoS_2-WS_2 is a reusable sensing material for gas detections.[59] Up to current analysis, we could conclude that MoS_2-WS_2 heterostructure is an outstanding resistive gas sensor toward CO and C_2H_2 with a favorable reliability at room temperature.

4. CONCLUSIONS

Based on the first-principles theory, this work uses a MoS_2-WS_2 heterostructure as a potential gas sensor upon two typical dissolved gases, CO and C_2H_2, in order to evaluate the operational status of oil-immersed transformers. It is found that the MoS_2-WS_2 heterostructure has much stronger adsorption performance and charge-transfer properties compared with isolated MoS_2 and WS_2, with the E_{ad} obtained as −0.15 and −0.25 eV and Q_T as −0.025 and −0.034 e, respectively. The electronic property of the MoS_2-WS_2 heterostructure is remarkably deformed giving rise to a more obvious change in the bandgap compared with the gas adsorbed MoS_2 or WS_2 systems. At room temperature, the sensing responses of the MoS_2-WS_2 are obtained as −99.56% and −99.95% for detection of CO and C_2H_2, and the recovery times are 0.34 and 16.84 ns for desorption of CO and C_2H_2. These findings manifest the strong potential of the MoS_2-WS_2 heterostructure as a favorable resistive and reusable gas sensor toward CO and C_2H_2, which paves the way to further explore the TMD-based heterostructure for gas sensing applications, typically for dissolved gas analysis in electrical oil-immersed transformers.

■ ASSOCIATED CONTENT

Supporting Information

The Supporting Information is available free of charge at https://pubs.acs.org/doi/10.1021/acsomega.4c00681.

Results of molecular dynamic simulations of MoS_2-WS_2 (Figure S1) (PDF)

■ AUTHOR INFORMATION

Corresponding Authors

Xiu Zhou − *Electric Power Research Institute, State Grid Ningxia Electric Power Co., Ltd, Ningxia 750001, China*; Email: zhouxiu007@163.com

Hao Cui − *Southwest University, Chongqing 400715, China*; orcid.org/0000-0002-9410-6345; Email: cuihaocqu@163.com

Authors

Tian Tian − *Electric Power Research Institute, State Grid Ningxia Electric Power Co., Ltd, Ningxia 750001, China*

Jiaying Yu − *Electric Power Research Institute, State Grid Ningxia Electric Power Co., Ltd, Ningxia 750001, China*

Jin Bai − *Electric Power Research Institute, State Grid Ningxia Electric Power Co., Ltd, Ningxia 750001, China*

Lei Chen − *Electric Power Research Institute, State Grid Ningxia Electric Power Co., Ltd, Ningxia 750001, China*

Ninghui He − *Electric Power Research Institute, State Grid Ningxia Electric Power Co., Ltd, Ningxia 750001, China*

Xiuguang Li − *Electric Power Research Institute, State Grid Ningxia Electric Power Co., Ltd, Ningxia 750001, China*

Heng Zhang − *Electric Power Research Institute, State Grid Ningxia Electric Power Co., Ltd, Ningxia 750001, China*

Complete contact information is available at: https://pubs.acs.org/10.1021/acsomega.4c00681

Notes

The authors declare no competing financial interest.

■ ACKNOWLEDGMENTS

This work is supported by Ningxia Natural Science Foundation (No. 2023AAC02083).

■ REFERENCES

(1) Cui, H.; Chen, D.; Zhang, Y.; Zhang, X. Dissolved gas analysis in transformer oil using Pd catalyst decorated $MoSe_2$ monolayer: A first-principles theory. *Sustainable Materials and Technologies* **2019**, *20*, No. e00094.

(2) Zhou, Q.; Zhang, G.; Tian, S.; Zhang, X. First-Principles Insight into Pd-Doped ZnO Monolayers as a Promising Scavenger for Dissolved Gas Analysis in Transformer Oil. *ACS Omega* **2020**, *5* (28), 17801−17807.

(3) Baek, D. H.; Kim, J. MoS_2 gas sensor functionalized by Pd for the detection of hydrogen. *Sensors & Actuators B Chemical* **2017**, *250*, 686−691.

(4) Lu, Y. C.; Wei, L.; Chao, W.; Peng, W. The New Development Trend of Distribution Transformer. *Applied Mechanics & Materials* **2014**, *672*−*674*, 831−836.

(5) Liao, R.; Zheng, H.; Grzybowski, S.; Yang, L.; Zhang, Y.; Liao, Y. An Integrated Decision-Making Model for Condition Assessment of Power Transformers Using Fuzzy Approach and Evidential Reasoning. *IEEE Transactions on Power Delivery* **2011**, *26* (2), 1111−1118.

(6) Singh, S.; Bandyopadhyay, M. N. Dissolved gas analysis technique for incipient fault diagnosis in power transformers: A bibliographic survey. *IEEE Electrical Insulation Magazine* **2010**, *26* (6), 41−46.

(7) He, X.; Gui, Y.; Xie, J.; Liu, X.; Wang, Q.; Tang, C. A DFT study of dissolved gas (C_2H_2, H_2, CH_4) detection in oil on CuO-modified BNNT. *Appl. Surf. Sci.* **2020**, *500*, 144030.

(8) Yang, F.; Jung, D.; Penner, R. M. Trace Detection of Dissolved Hydrogen Gas in Oil Using a Palladium Nanowire Array. *Anal. Chem.* **2011**, *83* (24), 9472−7.

(9) Ding, J.; Li, X.; Cao, J.; Sheng, L.; Yin, L.; Xu, X. New sensor for gases dissolved in transformer oil based on solid oxide fuel cell. *Sensors & Actuators B Chemical* **2014**, *202* (4), 232−239.

(10) Ma, G. M.; Li, C. R.; Luo, Y. T.; Mu, R. D.; Wang, L. High sensitive and reliable fiber Bragg grating hydrogen sensor for fault detection of power transformer. *Sensors & Actuators B Chemical* **2012**, *169* (8), 195−198.

(11) Benounis, M.; Aka-Ngnui, T.; Jaffrezic, N.; Dutasta, J. P. NIR and optical fiber sensor for gases detection produced by transformation oil degradation. *Sensors & Actuators A Physical* **2008**, *141* (1), 76−83.

(12) Zhang, G.; Zhang, X.; Cheng, H.; Tang, J. Ladder-wise calculation method for z-coordinate of transformer PD source based on planar layout UHF antenna sensors. *IEEJ. Transactions on Electrical and Electronic Engineering* **2020**, *15* (3), 340−345.

(13) Cui, H.; Zhang, G.; Zhang, X.; Tang, J. Rh-doped $MoSe_2$ as toxic gas scavenger: A first-principles study. *Nanoscale Advances* **2019**, *1* (2), 772−780.
(14) Cui, H.; Zhang, X.; Zhang, J.; Zhang, Y. Nanomaterials-based gas sensors of SF_6 decomposed species for evaluating the operation status of high-voltage insulation devices. *High Voltage* **2019**, *4* (4), 242−258.
(15) Sajjad, M.; Montes, E.; Singh, N.; Schwingenschlogl, U. Superior Gas Sensing Properties of Monolayer $PtSe_2$. *Advanced Materials Interfaces* **2017**, *4* (5), 1600911.
(16) Yang, H.; Wang, Z.; Ye, H.; Zhang, K.; Chen, X.; Zhang, G. Promoting sensitivity and selectivity of HCHO sensor based on strained InP_3 monolayer: A DFT study. *Appl. Surf. Sci.* **2018**, *459*, 554−561.
(17) Cui, H.; Ran, M.; Peng, X.; Zhang, G. First-principles design of noble metal (Rh and Pd) dispersed Janus WSTe monolayer for toxic gas sensing applications. *Journal of Environmental Chemical Engineering* **2024**, *12* (2), 112047.
(18) Zhang, D.; Yang, Z.; Li, P.; Pang, M.; Xue, Q. Flexible self-powered high-performance ammonia sensor based on Au-decorated $MoSe_2$ nanoflowers driven by single layer MoS_2-flake piezoelectric nanogenerator. *Nano Energy* **2019**, *65*, 103974.
(19) Shokri, A.; Salami, N. Gas sensor based on MoS_2 monolayer. *Sensors & Actuators B Chemical* **2016**, *236*, 378−385.
(20) Lin, Y.-F.; Xu, Y.; Wang, S.-T.; Li, S.-L.; Yamamoto, M.; Aparecido-Ferreira, A.; Li, W.; Sun, H.; Nakaharai, S.; Jian, W.-B.; Ueno, K.; Tsukagoshi, K. Ambipolar $MoTe_2$ Transistors and Their Applications in Logic Circuits. *Adv. Mater.* **2014**, *26* (20), 3263−3269.
(21) Cui, H.; Zhang, X.; Zhang, G.; Tang, J. Pd-doped MoS_2 monolayer: A promising candidate for DGA in transformer oil based on DFT method. *Appl. Surf. Sci.* **2019**, *470*, 1035−1042.
(22) Wu, E.; Xie, Y.; Yuan, B.; Zhang, H.; Hu, X.; Liu, J.; Zhang, D. Ultra-sensitive and Fully Reversible NO_2 Gas Sensing based on p-type $MoTe_2$ Under ultra-violet Illumination. *ACS Sensors* **2018**, *3*, 1719.
(23) Zhang, Y.; Yang, R.; Li, H.; Zeng, Z. Boosting Electrocatalytic Reduction of CO_2 to HCOOH on Ni Single Atom Anchored WTe2Monolayer. *Small* **2022**, *18* (44), 2203759.
(24) Xu, L.; Gui, Y.; Li, W.; Li, Q.; Chen, X. Gas-sensing properties of Pt_n-doped WSe_2 to SF_6 decomposition products. *Journal of Industrial and Engineering Chemistry* **2021**, *97*, 452−459.
(25) Srivastava, R.; Suman, H.; Shrivastava, S.; Srivastava, A. DFT analysis of pristine and functionalized zigzag CNT: A case of H_2S sensing. *Chem. Phys. Lett.* **2019**, *731*, 136575.
(26) Zhang, X.; Yu, L.; Wu, X.; Hu, W. Experimental Sensing and Density Functional Theory Study of H_2S and SOF_2 Adsorption on Au-Modified Graphene. *Advanced Science* **2015**, *2* (11), 612.
(27) Zhang, X.; Yu, L.; Gui, Y.; Hu, W. First-principles study of SF_6 decomposed gas adsorbed on Au-decorated graphene. *Appl. Surf. Sci.* **2016**, *367*, 259−269.
(28) Wang, G.; Yuan, H.; Chang, J.; Wang, B.; Kuang, A.; Chen, H. J. R. a. ZnO/MoX 2 (X = S, Se) composites used for visible light photocatalysis. *RSC Adv.* **2018**, *8* (20), 10828−10835.
(29) Wang, G.; Dang, S.; Zhang, P.; Xiao, S.; Wang, C.; Zhong, M. Hybrid density functional study on the photocatalytic properties of AlN/$MoSe_2$, AlN/WS_2, and AlN/WSe_2 heterostructures. *J. Phys. D: Appl. Phys.* **2018**, *51* (2), 025109.
(30) Zhang, D.; Yu, S.; Wang, X.; Huang, J.; Pan, W.; Zhang, J.; Meteku, B. E.; Zeng, J. J. J. o. H. M. UV illumination-enhanced ultrasensitive ammonia gas sensor based on (001) TiO_2/MXene heterostructure for food spoilage detection. *Journal of Hazardous Materials* **2022**, *423*, 127160.
(31) Chen, K.; Wan, X.; Xie, W.; Wen, J.; Kang, Z.; Zeng, X.; Chen, H.; Xu, J. J. A. m. Lateral built-in potential of monolayer MoS2-WS2 in-plane heterostructures by a shortcut growth strategy. *Advanced Materials* **2015**, *27* (41), 6431−6437.
(32) Sharma, A.; Mahlouji, R.; Wu, L.; Verheijen, M. A.; Vandalon, V.; Balasubramanyam, S.; Hofmann, J. P.; Kessels, W. M. M. E.; Bol, A. A. J. N. Large area, patterned growth of 2D MoS_2 and lateral MoS_2-WS_2 heterostructures for nano-and opto-electronic applications. *Nanotechnology* **2020**, *31* (25), 255603.
(33) Ikram, M.; Liu, L.; Liu, Y.; Ma, L.; Lv, H.; Ullah, M.; He, L.; Wu, H.; Wang, R.; Shi, K. J. J. o. M. C. A. Fabrication and characterization of a high-surface area MoS_2@WS_2 heterojunction for the ultra-sensitive NO_2 detection at room temperature. *J. Mater. Chem. A* **2019**, *7* (24), 14602−14612.
(34) Zhang, M.; Zhang, J. J. N. Highly Selective NH3 Sensor Based on MoS_2/WS_2 Heterojunction. *Nanomaterials* **2023**, *13* (12), 1835.
(35) Chen, D.; Zhang, X.; Xiong, H.; Li, Y.; Tang, J.; Xiao, S.; Zhang, D. A first-principles study of the SF_6 decomposed products adsorbed over defective WS_2 monolayer as promising gas sensing device. *IEEE Trans. Device Mater. Relib.* **2019**, *19* (3), 473−483.
(36) Zhang, D.; Wu, J.; Li, P.; Cao, Y. Room-temperature SO_2 gas-sensing properties based on a metal-doped MoS_2 nanoflower: an experimental and density functional theory investigation. *Journal of Materials Chemistry A* **2017**, *5* (39), 20666−20677.
(37) Cui, H.; Jia, P.; Peng, X. Adsorption of SO_2 and NO_2 molecule on intrinsic and Pd-doped $HfSe_2$ monolayer: A first-principles study. *Appl. Surf. Sci.* **2020**, *513*, 145863.
(38) Tkatchenko, A.; DiStasio, R. A., Jr.; Head-Gordon, M.; Scheffler, M. Dispersion-corrected Møller-Plesset second-order perturbation theory. *J. Chem. Phys.* **2009**, *131* (9), 171−171.
(39) Yang, A.; Pan, J.; Wang, D.; Lan, T.; Liu, Z.; Yuan, H.; Chu, J.; Wang, X.; Rong, M. Tunable SO_2-sensing performance of arsenene induced by Stone-Wales defects and external electric field. *Appl. Surf. Sci.* **2020**, *523*, 146403.
(40) Cui, H.; Yan, C.; Jia, P.; Cao, W. Adsorption and sensing behaviors of SF_6 decomposed species on Ni-doped C_3N monolayer: A first-principles study. *Appl. Surf. Sci.* **2020**, *512*, 145759.
(41) Ma, D.; Zeng, Z.; Liu, L.; Jia, Y. Theoretical screening of the transition metal heteronuclear dimer anchored graphdiyne for electrocatalytic nitrogen reduction. *Journal of Energy Chemistry* **2021**, *54*, 501−509.
(42) Gui, Y.; Shi, J.; Yang, P.; Li, T.; Tang, C.; Xu, L. Platinum modified MoS_2 monolayer for adsorption and gas sensing of SF_6 decomposition products: A DFT study. *High Voltage* **2020**, *5* (4), 454−462.
(43) Chaurasiya, R.; Dixit, A.; Pandey, R. Strain-mediated stability and electronic properties of WS_2, Janus WSSe and WSe_2 monolayers. *Superlattices & Microstructures* **2018**, *122*, 268−279.
(44) Pyykkö, P.; Atsumi, M. Molecular single-bond covalent radii for elements 1−118. *Chemistry* **2009**, *15* (1), 186−197.
(45) Tang, M.; Zhang, D.; Wang, D.; Deng, J.; Kong, D.; Zhang, H. Performance prediction of 2D vertically stacked MoS_2-WS_2 heterostructures base on first-principles theory and Pearson correlation coefficient. *Appl. Surf. Sci.* **2022**, *596*, 153498.
(46) Murphy, L. R.; Meek, T. L.; Allred, A. L.; Allen, L. C. Evaluation and test of pauling's electronegativity scale. *J. Phys. Chem. A* **2000**, *104* (24), 5867−5871.
(47) Ramaraj, S. G.; Nundy, S.; Zhao, P.; Elamaran, D.; Tahir, A. A.; Hayakawa, Y.; Muruganathan, M.; Mizuta, H.; Kim, S.-W. J. A. o. RF sputtered Nb-Doped MoS2 thin film for effective detection of NO_2 gas molecules: theoretical and experimental studies. *ACS Omega* **2022**, *7* (12), 10492−10501.
(48) Li, D.; Li, W.; Zhang, J. Al doped MoS_2 monolayer: a promising low-cost single atom catalyst for CO oxidation. *Appl. Surf. Sci.* **2019**, *484*, 1297−1303.
(49) Han, S. W.; Cha, G. B.; Park, Y.; Hong, S. C. Hydrogen physisorption based on the dissociative hydrogen chemisorption at the sulphur vacancy of MoS_2 surface. *Sci. Rep* **2017**, *7* (1), 7152.
(50) Gui, Y.; Peng, X.; Liu, K.; Ding, Z. Adsorption of C_2H_2, CH_4 and CO on Mn-doped graphene: Atomic, electronic, and gas-sensing properties. *Physica E: Low-dimensional Systems and Nanostructures* **2020**, *119*, 113959.
(51) Huang, J.; Chu, J.; Wang, Z.; Zhang, J.; Yang, A.; Li, X.; Gao, C.; Huang, H.; Wang, X.; Cheng, Y.; Rong, M. Chemisorption of NO_2 to MoS_2 Nanostructures and its Effects for MoS_2 Sensors. *ChemNanoMat* **2019**, *5* (9), 1123−1130.

https://doi.org/10.1021/acsomega.4c00681
ACS Omega 2024, 9, 20253−20262

(52) Shi, Z.; Zhang, J.; Zeng, W.; Zhou, Q. Adsorption and Sensing Performances of $MoTe_2$ Monolayers Doped with Pd, Ni, and Pt for SO_2 and NH_3: A DFT Investigation. *Langmuir* **2023**, *39* (11), 4125−4139.
(53) Cui, H.; Guo, Y.; Zhao, Q.; Zhang, G. Pd-doped $PtSe_2$ monolayer with strain-modulated effect for sensing SF_6 decomposed species: a first-principles study. *Journal of Materials Research and Technology* **2022**, *18*, 629−636.
(54) Tao, L.; Dastan, D.; Wang, W.; Poldorn, P.; Meng, X.; Wu, M.; Zhao, H.; Zhang, H.; Li, L.; An, B. J. A. A. M. Interfaces, Metal-decorated InN monolayer senses N_2 against CO_2. *ACS Appl. Mater. Interfaces* **2023**, *15* (9), 12534−12544.
(55) Wu, H.; Xia, Y.; Zhang, C.; Xie, S.; Wu, S.; Cui, H. Adsorptions of C5F10O decomposed compounds on the Cu-decorated NiS2 monolayer: a first-principles theory. *Mol. Phys.* **2023**, *121*, No. e2163715.
(56) Verlag, S. Semiconductor Physical Electronics. *Semiconductor Physical Electronics* **2006**, *28* (3), 363−364.
(57) Zhang, Y.-H.; Chen, Y.-B.; Zhou, K.-G.; Liu, C.-H.; Zeng, J.; Zhang, H.-L.; Peng, Y. Improving gas sensing properties of graphene by introducing dopants and defects: a first-principles study. *Nanotechnology* **2009**, *20* (18), 185504.
(58) Peng, S.; Cho, K.; Qi, P.; Dai, H. Ab initio study of CNT NO_2 gas sensor. *Chem. Phys. Lett.* **2004**, *387* (4), 271−276.
(59) Vadalkar, S.; Chodvadiya, D.; Som, N. N.; Vyas, K. N.; Jha, P. K.; Chakraborty, B. An Ab-initio Study of the C18 nanocluster for Hazardous Gas Sensor Application. *ChemistrySelect* **2022**, *7* (3), No. e202103874.

https://doi.org/10.1021/acsomega.4c00681
ACS Omega 2024, 9, 20253−20262